



HSPB seismic broadband station in Southern Spitsbergen: First results on crustal and mantle structure from receiver functions and SKS splitting

Monika WILDE-PIÓRKO¹, Marek GRAD^{1,2}, Paweł WIEJACZ²
and Johannes SCHWEITZER³

¹ Instytut Geofizyki, Uniwersytet Warszawski, Pasteura 7, 02-093 Warszawa, Poland
<mwilde@igf.fuw.edu.pl> <mgrad@mimuw.edu.pl>

² Instytut Geofizyki, Polska Akademia Nauk, Księcia Janusza 64, 01-452 Warszawa, Poland
<pwiejacz@igf.edu.pl>

³ NORSAR, Gunnar Randers vei 15, 2027-Kjeller, Norway *<johannes.schweitzer@norsar.no>*

Abstract: In the framework of the 4th International Polar Year Panel “Plate Tectonics and Polar Gateways” the international project “The Dynamic Continental Margin Between the Mid-Atlantic-Ridge System (Mohns Ridge, Knipovich Ridge) and the Bear Island Region” was undertaken in 2007–2008. As a part of this project a new three-component seismic broadband station was installed in September 2007 in the area of the Polish Polar Station Hornsund in Southern Spitsbergen. The new HSPB station has the coordinates: $\phi = 77.0019^\circ\text{N}$, $\lambda = 15.5332^\circ\text{E}$, $H = 11 \text{ m a.s.l.}$ During the first years of operation a number of good quality teleseismic events were recorded. This gives the opportunity for a first determination of crustal and mantle structure beneath the station by using receiver function (RF) and SKS splitting techniques. The Moho depth determined using RF is about 32 km beneath HSPB. Significant amplitudes on the transverse components of the RF indicate a shallowly dipping discontinuity (sedimentary-basement) towards the south-west. The fast polarization of SKS phases is near parallel to the border between the continental and the oceanic crust and the Hornsund fault ($\alpha = 151.8^\circ$). The average time delay δt between “fast” and “slow” directions is 0.68 s, which implies ca. 2% anisotropy in a 100–200 km thick layer in the mantle.

Key words: Arctic, Spitsbergen, HSPB broadband seismic station, receiver functions, SKS splitting, crustal and mantle structure.

Introduction

Spitsbergen is located in the Arctica, on the north-western part of the Barents Sea continental platform and is bordered to the west and to the north by passive continental margins with transition to oceanic crust (Fig. 1). In general this is an area of transition from 30–35 km thick continental crust in the east, to oceanic crust with Moho at 10–15 km depth in the west. The Hornsund Fault, the promi-

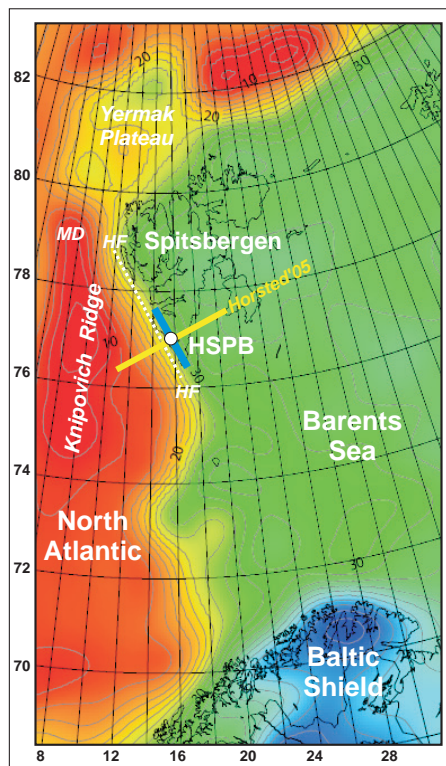


Fig. 1. Location of the HSPB seismic station (open circle) in Southern Spitsbergen on the background of the Moho depth map (Grad *et al.* 2009). The yellow line shows a part of the Horsted'05 seismic profile (Czuba *et al.* 2008; for crustal cross section see Fig. 10). Thick blue bar shows “fast” polarization of SKS phases which is near parallel to the border between the continental and oceanic crust ($\alpha = 151.8^\circ$). HF – Hornsund Fault; MD – Moloy Deep.

inent tectonic structure which parallels the Spitsbergen coast to the west, can be traced from Bjørnøya at ca. 75°N, to about 79°N (Sundvor and Eldholm 1979; Sundvor and Eldholm 1980; Fig. 1). The spreading axis in the Greenland Sea is today represented by the Knipovich Ridge. This is an area of interest because of its structure and geodynamic processes, however logistically difficult to access for detailed studies. This area was one of the subjects of the 4th International Polar Year Panel “Plate Tectonics and Polar Gateways”. The international project “The Dynamic Continental Margin Between the Mid-Atlantic-Ridge System (Mohns Ridge, Knipovich Ridge) and the Bear Island Region” focused on multi-disciplinary seismic studies (broadband long-term Ocean Bottom Seismometers (OBSs) and land stations, local seismicity, seismic refraction and reflection profiling), performed in two arctic summer seasons in 2007 and 2008 and during the winter 2007/2008. In the framework of this project a new permanent seismic broadband station was installed in September 2007 in the area of the Polish Polar Station Hornsund in Southern Spitsbergen. The station was installed by NOR-SAR and the

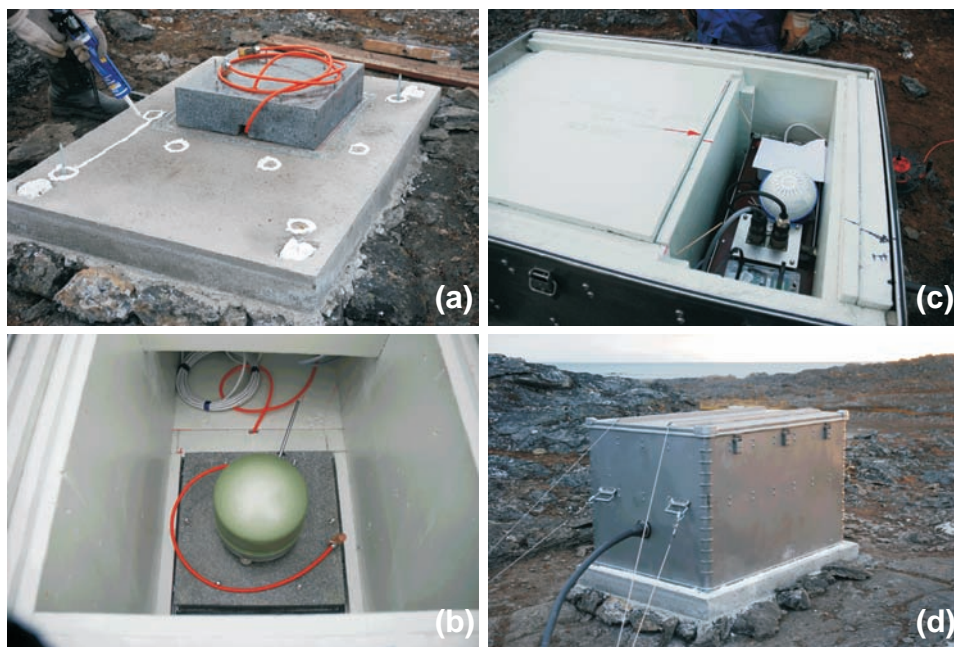


Fig. 2. Installation of the HSPB seismic broadband station in Southern Spitsbergen in September 2007. (a) basement preparation; (b) STS-2 seismometer installation; (c) completion of device; (d) HSPB station ready for operation.

Institute of Geophysics, Polish Academy of Sciences (which is now responsible for its operation, service and data transfer). The station was equipped with a three-component Streckeisen STS-2 seismometer and a Gürnalp CMG-DM24 data logger. The sensor was installed on a gabbro plate laying on a concrete plinth and protected against tilt, air pressure and temperature fluctuations by few layers of foamed polystyrene, a stainless steel helmet and an aluminium box (Fig. 2) following suggestions by Wielandt and Widmer-Schnidrig (2002). The power supply is coming from the ca. 300 m distant Polish Polar Station Hornsund. The data are sampled with 1, 0.1 and 0.01 s (corresponding to 1, 10 and 100 Hz) and sent by cable transmission to the Polish Polar Station Hornsund. The raw data are archived on DVD and external disc storage and sent approximately each month to NORSAR and to the Institute of Geophysics PAS. The new HSPB station has the coordinates: $\phi = 77.0019^\circ\text{N}$, $\lambda = 15.5332^\circ\text{E}$, $H = 11 \text{ m a.s.l.}$

Data

The installation of the broadband station at HSPB has raised the question on the quality of the recording. The best insight into the seismic noise level is rendered by the power spectral density $p(\tau)$ which is the Fourier transform of the autocorrelation

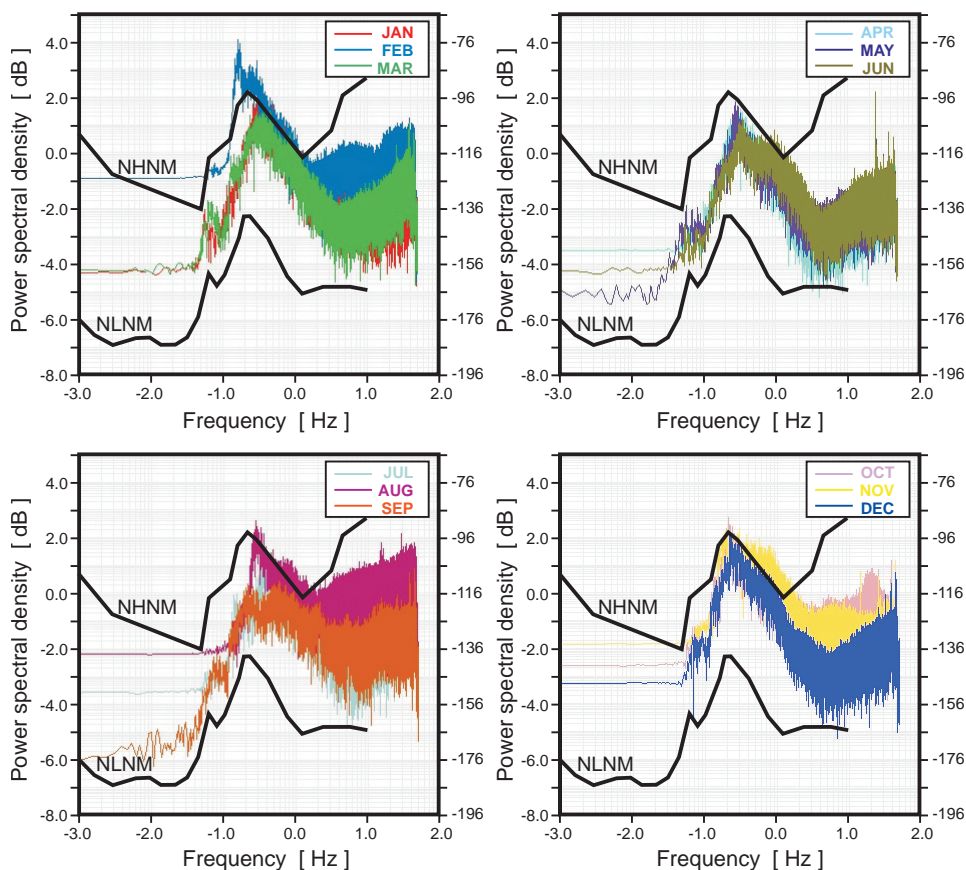


Fig. 3. Power spectral density for HSPB seismic station calculated from Z component for 10-minute time windows selected each month of 2008 year on the same days of the month and the same time of the day. New High and New Low Noise Model (NHNM and NLNM) are marked by thick black lines (Peterson, 1993). The scale of axes are logarithmic. The spectra are presented in units of decibels referred to 1 (counts)²/Hz (left side of plots) and 1 (m/s²)²/Hz (right side of plots).

function $p(t) = \langle f(t) \cdot f(t+\tau) \rangle$, where $f(t)$ is the seismic signal and the “ $\langle \dots \rangle$ ” denote averaging over time t (Havskov and Aguacil, 2004). Best visual effect is achieved in case of acceleration power spectral density, as the velocity and displacement power spectra usually fall off with frequency and thus are more difficult to perceive by eye.

The power spectra for HSPB have been calculated from Z component for 10-minute time windows selected each month on the same days of the month (13th) and the same time of the day (06:00–06:10 UT). Results are presented in Fig. 3. Generally the shape of the power spectra remains similar over the whole year with the exceptions of February and August. The high noise in August can be attributed to human activity around the HSPB Polar Base, increased while seasonal summer activities, in particular repairs and construction are in progress. The high noise in February is most likely caused by a stretch of extremely bad weather. Apart from

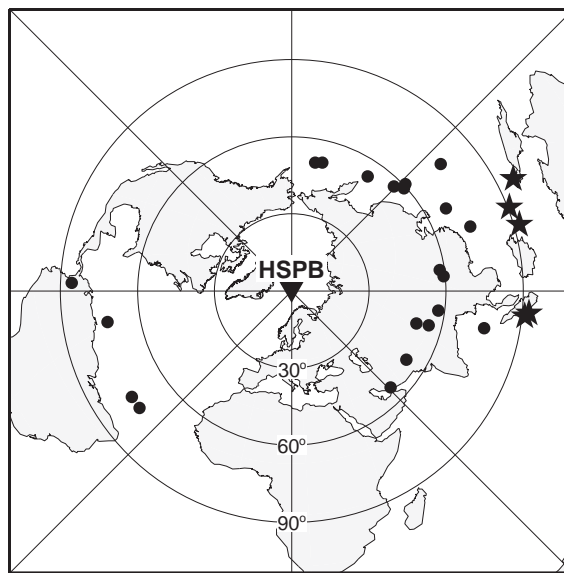


Fig. 4. Distribution of events used in this study. The azimuthal-equidistant projection shows the true distances and backazimuths of the epicenters with respect to the HSPB seismic station ($\phi = 77.0019^\circ\text{N}$, $\lambda = 15.5332^\circ\text{E}$, $H = 11 \text{ m a.s.l.}$). Dots are epicentres of events used in RF technique, stars are epicentres of events used for SKS phase splitting.

those two months, noise level at HSPB falls to mid-way between the High and Low Noise Model (Peterson 1993). This result could have been anticipated for a site that is away from sources of cultural noise but located a few hundred meters from the sea and exposed to gusts of wind.

The HSPB broadband station began operation in late September 2007. In this paper we use selected seismograms recorded before the end of February 2009. Although it is a short time interval of about 18 months, a number of good quality teleseismic events were recorded. Details for all used events were put together in Table 1, and their epicentres are shown in Fig. 4. For the SKS phase splitting analysis 5 good quality events were selected with magnitude $M > 6.8$ in the epicentral distance interval $91\text{--}97^\circ$ (area of Indonesia). Examples of seismograms used in the SKS phase splitting analysis are shown in Fig. 5. For the P-wave receiver function analysis 23 events were selected with magnitude $M > 6.0$ in the epicentral distance interval $30\text{--}92^\circ$. Most of events are concentrated in the backazimuth range $13\text{--}135^\circ$, however 4 events from the western hemisphere were also used (backazimuth $232\text{--}273^\circ$). Examples of seismograms used in P-wave RF analysis are shown in Fig. 6.

Receiver function technique and crustal model

The receiver function technique were first applied to data recorded at the World-Wide Standard Seismograph Network station LON (Longmire, Washington)

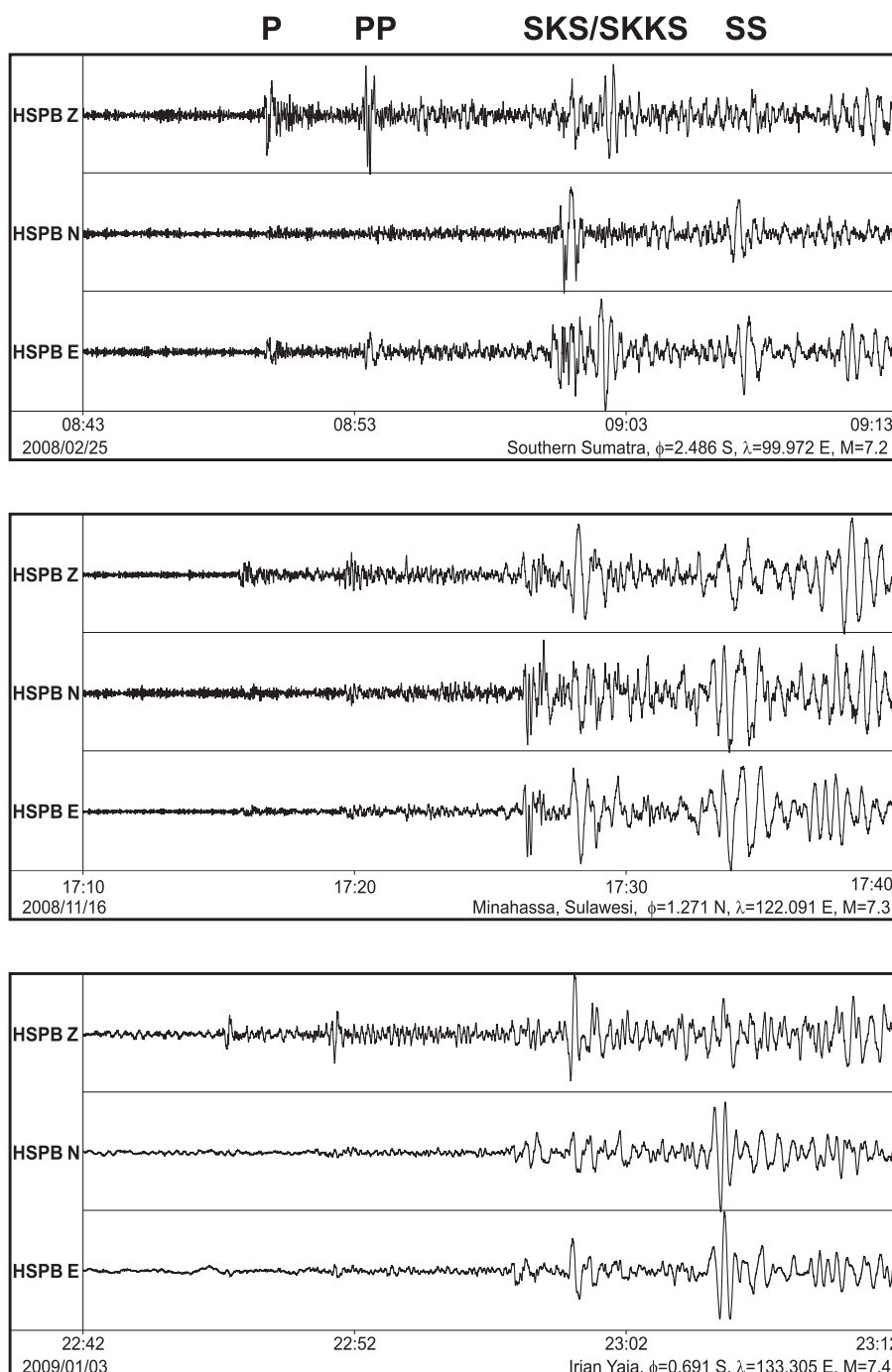


Fig. 5. Examples of unfiltered three-component seismograms (Z, N, E) for three teleseismic earthquakes recorded at HSPB station used for the SKS phase splitting study. Each seismogram shows 30 minute records; the phases P, PP, SKS/SKKS and SS are marked. See Table 1 for details.

Table 1

List of events used for the P-wave RF (No. 1–23) and SKS phase splitting (No. 24–28) analysis. Focal parameters are taken from USGS/NEIC PDE Catalogue. The two right side columns show results of the SKS phase splitting: fast direction α and time delay δt .

No	Date [yr/mm/dd]	Time [hr:min:s]	Lat. [°]	Lon. [°]	Depth [km]	Mag. M	Dist. [°]	Bazm. [°]	α [°]	δt [s]
1	2007/09/28	13:38:57.9	22.01 N	142.67 E	260	7.5	76.2	49.6	—	—
2	2007/11/29	19:00:20.4	14.94 N	61.27 W	156	7.4	72.5	260.5	—	—
3	2008/02/25	08:36:33.0	2.49 S	99.97 E	25	7.2	91.2	96.0	—	—
4	2008/03/20	22:32:57.9	35.49 N	81.47 E	10	7.2	50.2	104.6	—	—
5	2008/05/02	01:33:37.2	51.86 N	177.53 W	14	6.6	50.9	10.4	—	—
6	2008/05/12	06:28:01.6	31.00 N	103.32 E	19	7.9	59.4	84.4	—	—
7	2008/05/20	13:53:35.6	51.16 N	178.76 E	27	6.3	51.4	13.4	—	—
8	2008/05/23	19:35:34.8	7.31 N	34.90 W	8	6.5	74.6	232.5	—	—
9	2008/06/01	01:57:23.7	20.12 N	121.35 E	31	6.3	73.9	70.1	—	—
10	2008/06/13	23:43:45.4	39.03 N	140.88 E	7	6.9	59.2	47.6	—	—
11	2008/06/27	11:40:14.0	11.01 N	91.82 E	17	6.6	76.2	100.9	—	—
12	2008/07/08	07:42:10.7	27.53 N	128.33 E	43	6.0	68.1	61.8	—	—
13	2008/07/19	02:39:28.7	37.55 N	142.21 E	22	7.0	60.8	46.7	—	—
14	2008/07/21	11:30:29.3	37.19 N	142.05 E	22	6.0	61.2	47.0	—	—
15	2008/08/05	09:49:17.3	32.76 N	105.49 E	6	6.0	58.2	81.8	—	—
16	2008/08/25	13:21:58.8	30.90 N	83.52 E	12	6.7	55.1	104.0	—	—
17	2008/09/10	11:00:34.1	26.74 N	55.83 E	12	6.1	53.7	134.3	—	—
18	2008/09/10	13:08:14.9	8.09 N	38.72 W	10	6.6	74.5	236.5	—	—
19	2008/09/11	00:20:50.9	41.89 N	143.75 E	25	6.8	56.8	44.3	—	—
20	2008/09/13	09:32:01.5	4.79 N	75.52 W	132	5.7	85.6	272.1	—	—
21	2008/10/06	08:30:45.6	29.81 N	90.35 E	12	6.3	57.6	97.5	—	—
22	2008/10/29	11:32:43.1	30.60 N	67.46 E	14	6.4	52.0	120.7	—	—
23	2009/01/15	17:49:39.1	46.86 N	155.15 E	36	7.4	53.6	33.4	—	—
24	2007/10/24	21:02:50.6	3.90 S	101.02 E	21	6.8	92.8	95.3	167.7	0.76
25	2008/02/25	08:36:33.0	2.49 S	99.97 E	25	7.2	91.2	96.0	164.4	0.38
26	2008/11/16	17:02:32.7	1.27 N	122.09 E	30	7.3	92.4	73.6	154.4	1.12
27	2009/01/03	22:33:40.3	0.69 S	133.30 E	23	7.4	96.7	63.0	130.7	0.08
28	2009/02/11	17:34:50.8	3.88 N	126.40 E	22	7.2	90.8	68.8	141.8	1.05

by Langston (1979) and since that time it is still being developed (*e.g.* Owens *et al.* 1984; Cassidy 1992; Kind *et al.* 1995). A receiver function calculated from teleseismic P-waves contains only information about the structure beneath the station. Ammon (1991) has shown that the receiver function for a one-dimensional structure can be written as a scaled version of the radial component of the seismogram with P multiples removed. For a teleseismic P-wave (Fig. 7a) impinging on a stack of horizontal homogeneous layers beneath the station we should not observe any seismic

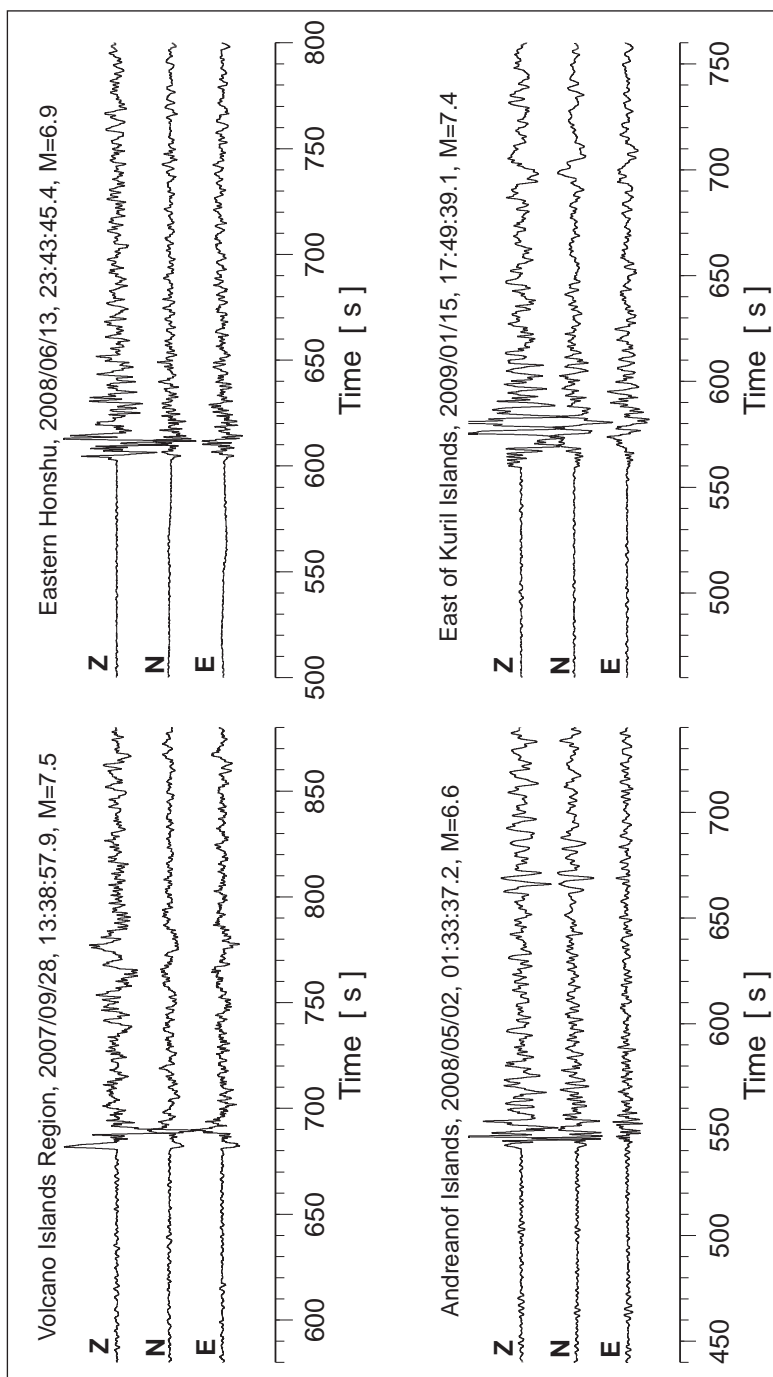


Fig. 6. Examples of unfiltered three-component seismograms (Z, N, E) for four teleseismic earthquakes recorded at the HSPB station used in the RF study. Each seismogram shows 300 s long records; time in seconds from origin of event. See Table 1 for details.

energy on the tangential component of the seismogram. The receiver function for one-dimensional structures contains only the P-to-S converted phases with P multiples removed (Fig. 7b). Their arrival times (calculated relative to the arrival of the direct P-wave) depend on the depth of the discontinuities and the S-wave velocity in the layers. Amplitudes of the receiver function depend on the contrast of seismic velocities at the boundary. These results are also valid for more complicated laterally homogeneous media with dipping discontinuities. But in this case, the energy of the converted waves also contributes to the tangential component (Cassidy 1992). What is more, we can observe very typical azimuthal variation of the radial and the tangential receiver functions caused by dipping discontinuities (Fig. 7c) without any energy on the tangential receiver function for waves travelling in the downdip or updip direction of the discontinuity. The amplitudes of the converted phases also change their signs in reference to the downdip and updip direction. That can allow us to estimate the value of the strike of dipping interface.

The HSPB seismograms of P-waves from teleseismic events in the distance range 30–92° were rotated into L , Q and T components, cut into time windows 10 s before and 80 s after the first arrival of P waves calculated from the *iasp91* model (Kennett and Engdahl 1991). Then, the Q and T components were deconvolved with the L components of seismograms, respectively in the frequency domain after applying a *water-level* correction with *water-level* parameter equal 0.01 and the high frequencies within the signals were suppressed using a lowpass Gaussian filter with a parameter of 2 (frequencies up to about 1 Hz). Additionally, a normalization procedure is applied which preserves the absolute amplitude information (Ammon 1991). The results of the component divisions, the *water-level* procedure and the Gaussian filtering are then transformed back to time-domain by Inverse Fourier Transform. Each receiver function was then moveout corrected for a slowness of 6.4 s/°. Fig. 8 shows the stacked Q (RFQ) and T (RFT) components of the receiver functions in 18 slowness bins of 0.17 s/° wide (Fig. 8a) and in 18 backazimuth bins of 20° wide (Fig. 8b). The overlapping of the bins in each case were 50%. The change of the shape of the receiver functions with slowness and backazimuth is clearly visible. For example there is a big difference in amplitudes and signal width of phases converted from the Moho discontinuity for teleseismic events from south-west and north-east (RFQ , Fig. 8b). This is a clear indication that the structure beneath the seismic station must differ depending on the backazimuth direction. We can observe very clear P-to-S conversions from the Moho discontinuity at about 4.5 s (4.2–4.8 s) and strong converted phases from the upper crust at about 1 s (0.8–1.3 s) on RFQ (Fig. 8). The tangential receiver functions show strong signal and backazimuthal dependence. We can observe very strong converted phases on RFT generated in the upper crust at about 1 s, which change its sign with respect to the backazimuth (Fig. 8b). Phases on the tangential receiver functions point to the existence of dipping discontinuities beneath the station or anisotropy of the structure or both. These two effects have different influences on the backazimuthal variation of the tangential receiver functions.

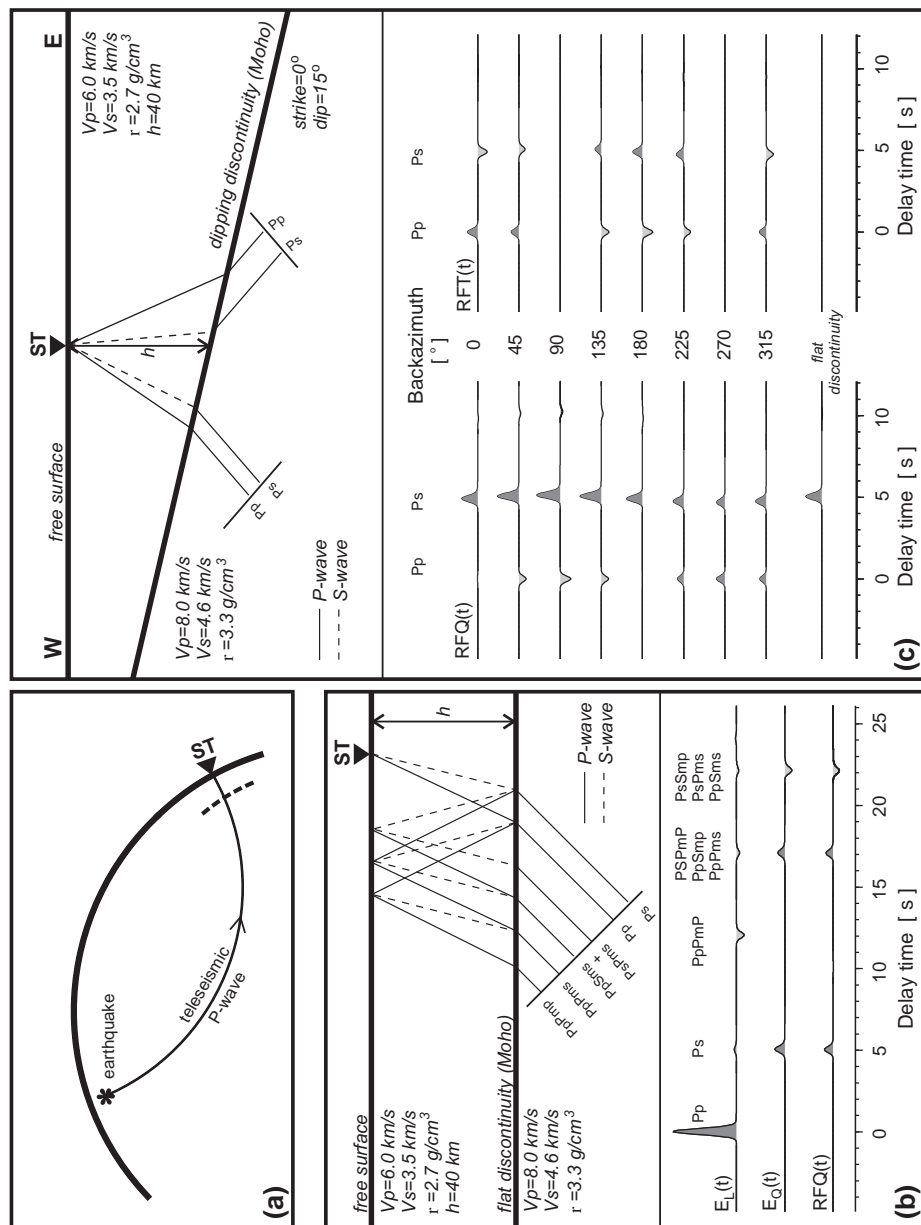


Fig. 7. Explanations for the RF technique. (a) Telesismic P-wave impinging on horizontal discontinuity beneath a seismic station. (b) Conversion of seismic waves at the discontinuity beneath a seismic station. The upper case letters denote upgoing waves, the lower case letters downgoing ones and m indicates the reflection from the Moho discontinuity. At the bottom are shown corresponding $E_L(t)$ and $E_Q(t)$ structure response and its receiver function for the model shown above. (c) Conversion of seismic waves for updip and downdip directions at the eastward dipping discontinuity beneath the seismic station. At the bottom are shown the corresponding Q (RFQ) and T (RFT) components of the receiver functions for a dipping discontinuity (different backazimuth) and for comparison RFs for a horizontal discontinuity, respectively.

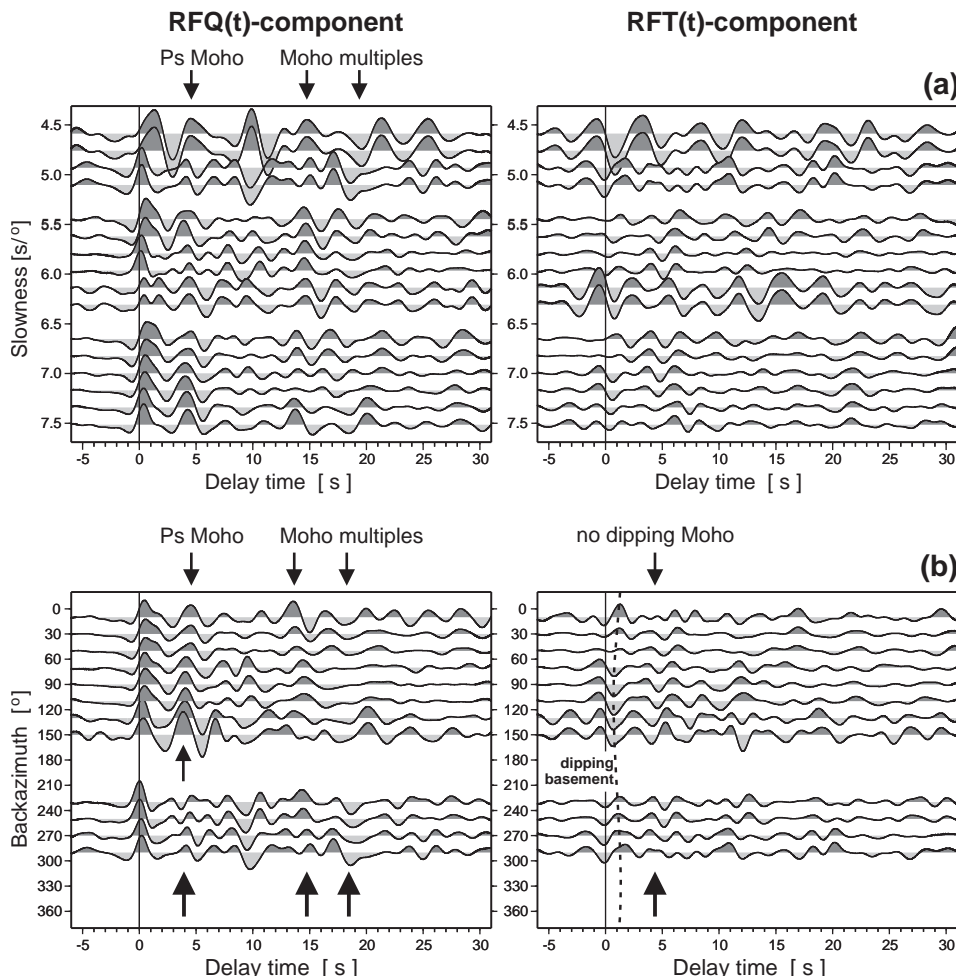


Fig. 8. Stacked receiver functions (RFQ and RFT components) for the HSPB station, sorted versus slowness (a) and backazimuth (b). The amplitude scale is the same for all components. Time zero refers to the direct P phase. The P-to-S conversion phases from the Moho discontinuity (Ps Moho) and associated multiples from the Moho and reflection at the free surface (Moho multiples) are marked by arrows. Converted phases from a dipping discontinuity in the upper crust are marked by dashed line. See text for further explanation.

The preliminary investigation (based on Fig. 7c) points to the existence of a dipping discontinuity (sediments–basement) in the south-west direction at the depth about 7 km beneath the HSPB station.

We can observe also clear conversions on RFQ in time interval 13.8–14.8 s (positive amplitudes) and 17.5–19.5 s (negative amplitudes) associated with multiples from the Moho discontinuity and the free surface (Fig. 8a). Using this information, we can estimate an average crustal Poisson's ratio σ and Moho depth z_m following the approach of Zhu and Kanamori (2000). In a grid search over the

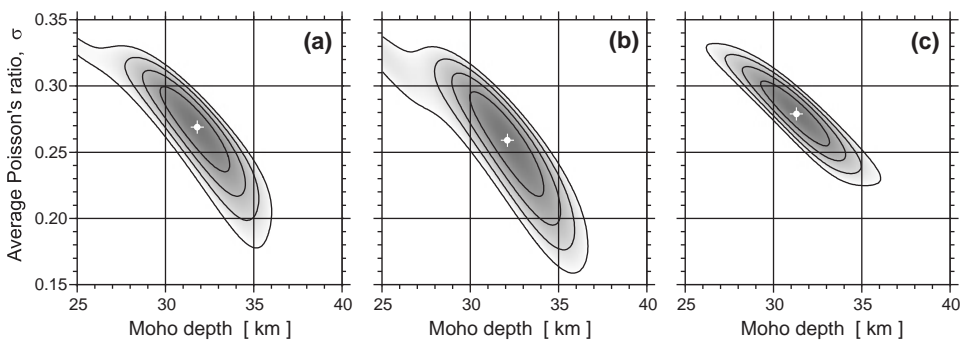


Fig. 9. Results of simultaneous Moho depth z_m and Poisson's ratio σ determination using the method of Zhu and Kanamori (2000) for (a) all events used in the receiver function analysis (23 events), (b) events from north-east (backazimuth $13\text{--}135^\circ$; 19 events) and (c) events from south-west (backazimuth $232\text{--}273^\circ$, 4 events). The optimum value was found by a grid search within a depth interval of 25–40 km and an interval for the Poisson's ratio of 0.15–0.35. Amplitudes are normalized in the range from 0 to 1. White areas correspond to low amplitudes (0–0.6), grey correspond to fits better than 0.6, and the white crosses in the darkest areas show the best fits.

σ - z_m space, we can determine the (σ, z_m) pair, which is in closest agreement with the observed Ps, PsPmP+PpSmP and PsSmP waveforms. The method was found to be very sensitive to the average Poisson's ratio in the crust but it works only in the cases if a clear Moho conversion and their associated multiples are observed (*e.g.* Kumar *et al.* 2001). This could be achieved through low-pass filtering, which enhances the multiples through reduction of most of the incoherent (high-frequency) energy. For the stack of all events the average crustal Poisson's ratio is 0.269 ± 0.021 and Moho depth is 31.8 ± 1.3 km (Fig. 9). Calculations performed separately for events from the north-east and south-west backazimuths show that the average crustal Poisson's ratio is 0.259 ± 0.028 and 0.279 ± 0.007 , respectively and the Moho depth is 32.1 ± 1.5 km and 31.3 ± 0.6 km, respectively.

We can compare our results with a 2-D seismic model obtained along the profile Horsted'05 (Czuba *et al.* 2008). The south-western part of this model is shown in Fig. 10. Below station HSPB (at ~ 75 km of profile) sedimentary layers with a P-wave velocity in the order of 5.3 km/s reach the depth of 5 km. The upper crustal layer with velocities 6.1–6.2 km/s dips down to 17 km. Below is the lower crust with velocities 6.7–7.1 km/s with variable thickness from 2–4 km at the ends of the profile and 17 km at 70 km of the model. The Moho depth in the SW part of the model shallows up to 14 km, while beneath the Polish Polar Station Hornsund it dips down to 33 km. Further to the East the model is rather simple, with two layers: in the upper crust P-wave velocity is in the order of 5.6–6.1 km/s, and in the lower crust a P-wave velocity is 6.1–6.2 km/s. There is no P-wave velocity higher than 6.5 km/s in the continental crust of central Spitsbergen. The P-wave velocity below the Moho interface is generally 8.05 km/s lowering to 7.95 km/s in the western part of the model. Additionally, an upper mantle reflector was found at a depth of about 40 km.

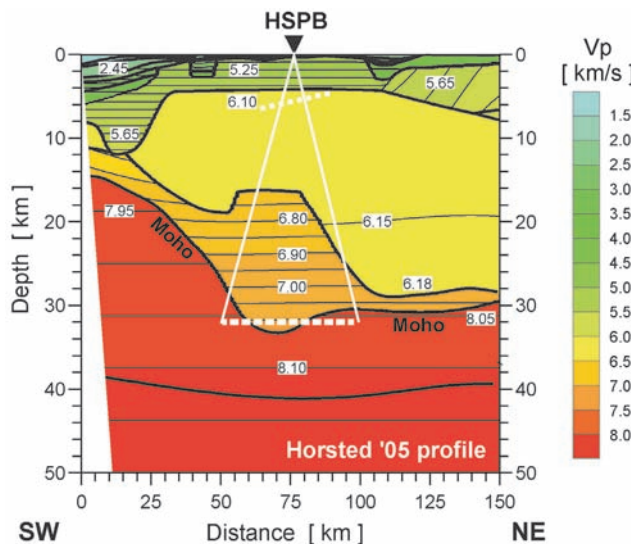


Fig. 10. Two-dimensional seismic P-wave velocity model along the south-western part of the Horsted '05 profile modelled by raytracing (Czuba *et al.* 2008). Black lines represent seismic discontinuities (boundaries); numbers in the model are the P-wave velocities in km/s. The triangle shows the location of the station HSPB. Vertical exaggeration is 3:1. The white broken lines show the results of RF studies: south-west dipping basement (at about 7 km depth) and a Moho depth beneath the station of about 32 km.

The crustal structure beneath the HSPB station obtained from the deep seismic sounding investigation is complicated and azimuthally dependent, which is confirmed by our receiver function study. The depth of the Moho discontinuity estimated from the Zhu and Kanamori method is close to the results obtained by Czuba *et al.* (2008). The sediment–basement discontinuity is most probably not horizontal but dipping in a south-west direction (Fig. 10). We are not able to see converted phases from the boundary between the upper and lower crust on the receiver function sections, most probably they are covered by multiple phases from the sediment–basement discontinuity. The contrasts in the seismic velocity at the sediment–basement and the Moho discontinuities are the strongest, so phases converted from these boundaries are best visible on receiver function sections. Unfortunately, there are not yet enough teleseismic events from north-west and south-east directions to investigate in more detail the 3-D seismic structure beneath the HSPB station.

SKS phase splitting

The installation of a new broadband station at HSPB permits an insight into the anisotropy of the mantle beneath the station (Vinnik *et al.* 1992), which was not possible with the earlier short period station data. However, the proximity of the sea and sea-related noise has limited the study to a few earthquakes with magnitudes above 6.8 thus leaving 5 events, all from the Indonesia to Philippines region.

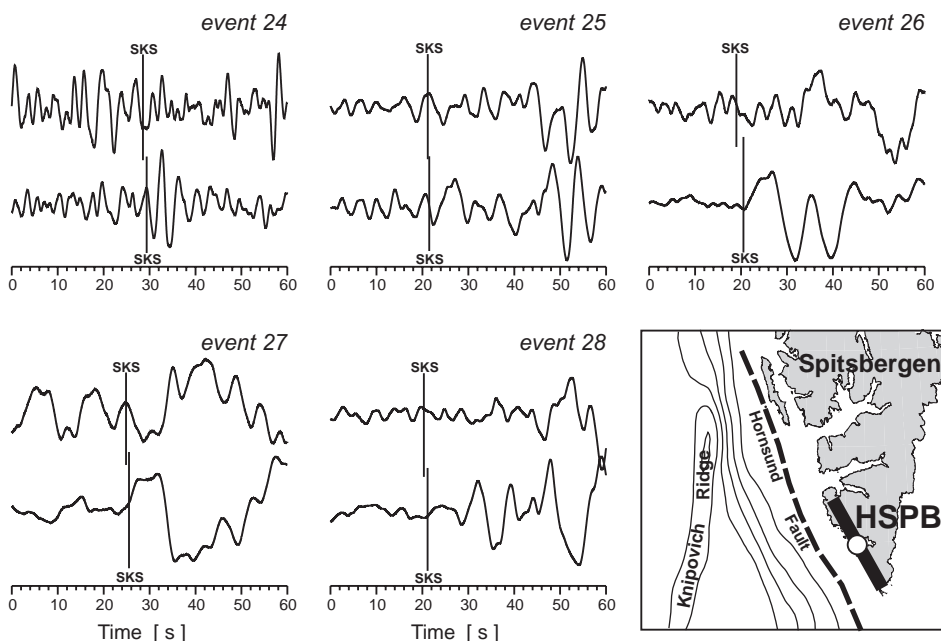


Fig. 11. Determination of delay time δt between “fast” (upper seismogram) and “slow” (lower seismogram) of SKS waves for earthquakes described in position No. 24–28, Table 1. All traces are cut in 60 second time window including SKS waves, normalized separately and filtered with standard third order Butterworth bandpass filter between 3 and 30 seconds. Average “fast” direction of SKS phases is marked by thick black bar on the background of the map of southern Spitsbergen.

The method used was similar to the one used by Wiejacz (2001) in a study of SKS splitting at broadband seismic stations in Poland, only the splitting algorithm that was part of the *Seismic Handler program* has been replaced by the shear wave splitting program of Ivan *et al.* (2008). For calculation of the splitting parameters a standard third order Butterworth bandpass filter between 3 and 30 seconds was applied to the seismic signals.

The fast directions of the split waves obtained from the 5 earthquake signals are in fair accord with each other, falling between 130.7° and 167.7° backazimuth – the results are presented in Table 1, positions 24–28. The average of the estimated fast directions is 151.8° with a standard error of 7.7° . The average fast direction is marked by thick blue bar on Fig. 1 and thick black bar Fig. 11. The determined delay times δt between the “fast” and the “slow” SKS waves varies in a relatively broad range, from 0.08 to 1.12 s (Fig. 11; Table 1), with an average of 0.68 s. The obtained azimuth of the fast split wave direction is parallel to the continent-ocean transition, and follows the direction of the Hornsund Fault. This result was not unexpected because the fast wave direction has previously been observed parallel to the trend of the rift (*e.g.*, Ethiopian Rift – Kendall *et al.* 2005). The observed average time delay $\delta t = 0.68$ s between “fast” and “slow” directions can be explained by ca. 2% anisotropy in a 100–200 km thick layer in the mantle (*e.g.*, Liu *et al.* 1995).

Conclusions

During 18 months of operation the new HSPB broadband seismic station in Southern Spitsbergen, Svalbard Archipelago provided teleseismic data for preliminary receiver function and SKS phase splitting studies. We have obtained some elements of the crustal and mantle structures: the depth of the Moho discontinuity (about 32 km) which is similar to previous studies; new features are the south-west inclined basement, the azimuth of the fast direction of SKS phase parallel to the continent-ocean transition ($\alpha = 151.8^\circ$) and the average time delay δt between “fast” and “slow” directions (0.68 s). However, to investigate in more detail the 3-D seismic structure beneath the station HSPB, a longer observation of teleseismic events is necessary.

Acknowledgements. — The paper was done in the framework of the 4th International Polar Year Panel “Plate Tectonics and Polar Gateways”, the international project “The Dynamic Continental Margin Between the Mid-Atlantic-Ridge System (Mohns Ridge, Knipovich Ridge) and the Bear Island Region”. We are very grateful to M.Sc. Eng. Jurek Suchcicki, M.Sc. Eng. Marian Hościłowicz, Assoc. Professor Piotr Glowacki and Professor Aleksander Guterch for installation of HSPB station. The equipment for the new broadband station at HSPB was financed by the Norwegian Research Council (NFR Project number 176069/S30). The public domain GMT software (Wessel and Smith 1995a; Wessel and Smith 1995b) has been used to produce some of the figures. The AH++ package written by Dr. Joachim Saul has been used for calculation of receiver functions. We thank very much reviewers Dr. Richard England and Dr. Sverker Olsson for their reviews and their valuable comments.

References

- AMMON C.J. 1991. The isolation of receiver effects from teleseismic P waveforms. *Bulletin of the Seismological Society of America* 81: 2504–2510.
- CASSIDY J.F. 1992. Numerical Experiment in Broadband Receiver Function Analysis. *Bulletin of the Seismological Society of America* 82: 1453–1474.
- CLAYTON R.W. and WIGGINS R.A. 1976. Source shape estimation and deconvolution of teleseismic bodywaves. *Geophysical Journal of the Royal Astronomical Society* 47: 151–177.
- CZUBA W., GRAD M., GUTERCH A., MAJDAŃSKI M., MALINOWSKI M., MJELDE R., MOSKALIK M., ŚRODA P., WILDE-PIÓRKO M. and NISHIMURA Y. 2008. Seismic crustal structure along the deep transect Horsted'05, Svalbard. *Polish Polar Research* 29 (3): 279–290.
- GRAD M., TIIRA T., BEHM M., BELINSKY A.A., BOOTH D.C., BRÜCKL E., CASSINIS R., CHADWICK R.A., CZUBA W., EGORKIN A.V., ENGLAND R.W., ERINCHEK Yu.M., FOUGLER G.R., GACZYŃSKI E., GOSAR A., GUTERCH A., HEGEDÚS E., HRUBCOVÁ P., JANIK T., JOKAT W., KARAGIANNI E.E., KELLER G.R., KELLY A., KOMMINAHO K., KORJA T., KORSTRÖM J., KOSTYUCHENKO S.L., KOZLOVSKAYA E., LASKE G., LENKEY L., LUOSTO U., MAGUIRE P.K.H., MAJDAŃSKI M., MALINOWSKI M., MARONE F., MECHIE J., MILSHTEIN E.D., MOTUZA G., NIKOLOVA S., OLSSON S., PASYANOS M., PETROV O.V., RAKITOV V.E., RAYKOVA R., RITZMANN O., ROBERTS R., SACHPAZI M., SANINA I.A., SCHMIDT-AURSCH M.C., SERRANO I., ŠPIČÁK A., ŚRODA P., ŠUMANOVAC F., TAYLOR B., TIIRA T., VEDRENTSEV A.G., VOZÁR J., WEBER Z., WILDE-PIÓRKO M., YEGOROVA T.P., YLINIEMI J., ZELT B. and ZOLOTOV E.E.

2009. The Moho depth map of the European Plate. *Geophysical Journal International* 176: 279–292. doi:10.1111/j.1365-246X.2008.03919.x
- HAVSKOV J. and AGUACIL G. 2004. *Instrumentation in Earthquake Seismology*. Springer, Berlin: 360 pp.
- IVAN M., POPA M. and GHICA D. 2008. SKS splitting observed at Romanian broad-band seismic network. *Tectonophysics* 462: 89–98. doi:10.1016/j.tecto.2007.12.015
- KENDALL J.-M., STUART G.W., EBINGER C.J., BASTOW I.D. and KEIR D. 2005. Magma-assisted rifting in Ethiopia. *Nature* 433: 146–148. doi:10.1038/nature03161 PMid:15650736
- KENNEDY B.L.N. and ENGDAHL E.R. 1991. Traveltimes for global earthquakes location and phase identification. *Geophysical Journal International* 105: 429–465. doi:10.1111/j.1365-246X.1991.tb06724.x
- KIND R., KOSAREV G.L. and PETERSEN N.V. 1995. Receiver functions at the stations of the German Regional Seismic Network (GRSN). *Geophysical Journal International* 121: 191–202. doi:10.1111/j.1365-246X.1995.tb03520.x
- KUMAR M.R., SAUL J., SARKAR D., KIND R. and SHUKLA A.K. 2001. Crustal structure of the Indian Shield: New constraints from teleseismic receiver functions. *Geophysical Research Letters* 28: 1339–1342. doi:10.1029/2000GL012310
- LANGSTON C.A. 1979. Structure under Mount Rainier, Washington, inferred from teleseismic body waves. *Journal of Geophysical Research* 84: 4749–4762. doi:10.1029/JB084iB09p04749
- LIU H., DAVIS P.M. and GAO S. 1995. SKS splitting beneath southern California. *Geophysical Research Letters* 22: 767–770. doi:10.1029/95GL00487
- OWENS T.J., ZANDT G. and TAYLOR S.R. 1984. Seismic Evidence for an Ancient Rift Beneath the Cumberland Plateau, Tennessee: A Detailed Analysis of Broadband Teleseismic P Waveforms. *Journal of Geophysical Research* 89: 7783–7795. doi:10.1029/JB089iB09p07783
- PETERSON J. 1993. Observations and modelling of background seismic noise. *Open-file Report* 93-322, U.S. Geological Survey, Albuquerque, New Mexico: 94 pp.
- SUNDVOR E. and ELDHOLM O. 1979. The western and northern margin off Svalbard. *Tectonophysics* 59: 239–250. doi:10.1016/0040-1951(79)90048-9
- SUNDVOR E. and ELDHOLM O. 1980. The continental margin of the Norwegian-Greenland Sea: Recent and outstanding problems. *Transactions of the Royal Society of London, Series A* 294: 77–82. doi:10.1098/rsta.1980.0014
- VINNIK L.P., KRISHNA V.G., KIND R., BORMANN P. and STAMMLER K. 1994. Shear wave splitting in the records of the German Regional Seismic Network. *Geophysical Research Letters* 21: 457–460. doi:10.1029/94GL00396
- VINNIK L.P., MAKEYEVA L.I., MILEV A. and USENKO A.Y. 1992. Global patterns of azimuthal anisotropy and deformations in the continental mantle. *Geophysical Journal International* 111: 433–447. doi:10.1111/j.1365-246X.1992.tb02102
- WESSEL P. and SMITH W.H.F. 1995a. The Generic Mapping Tools GMT Version 3. *Technical Reference and Cookbook*: 77 pp.
- WESSEL P. and SMITH W.H.F. 1995b. *GMT Version 3*. Reference Manual Pages.
- WIEJACZ P. 2001. Shear wave splitting across Tornquist-Tesseyre zone in Poland. *Journal of Balkan Geophysical Society* 4: 91–100.
- WIELANDT P. and WIDMER-SCHNIDRIG R. 2002. Seismic sensing and data acquisition in the GRSN. In: M. Korn (ed.) *Ten Year of German Regional Seismic Network (GRSN)*. Wiley, John & Sons, Weinheim: 73–101.
- ZHU L. and KANAMORI H. 2000. Moho depth variation in southern California from teleseismic receiver functions. *Journal of Geophysical Research* 105: 2969–2980. doi:10.1029/1999JB900322

Received 30 June 2009

Accepted 2 October 2009